

PAPER • OPEN ACCESS

Electrode optimization of an electret-based vibration generator in slot-effect configuration

To cite this article: Cuong Phu Le and Einar Halvorsen 2018 *J. Phys.: Conf. Ser.* **1052** 012117

View the [article online](#) for updates and enhancements.

Related content

- [Equivalent-circuit model for slot-effect configuration of an electret-based generator](#)
Cuong Phu Le, Michael Renaud and Einar Halvorsen
- [A 3-way pushable electret-based energy harvester fabricated with 3d-printing and PDMS molding](#)
Y. F. Chen, H. Honma and H. Toshiyoshi
- [Optimal geometry of a parallelized electret-based vibration energy harvester](#)
H Okamoto, Y Hamate, L Xu et al.



IOP | ebooks™

Bringing you innovative digital publishing with leading voices to create your essential collection of books in STEM research.

Start exploring the collection - download the first chapter of every title for free.

Electrode optimization of an electret-based vibration generator in slot-effect configuration

Cuong Phu Le and Einar Halvorsen

Department of Microsystems, University College of Southeast Norway, Campus Vestfold,
Raveien 215, 3184 Borre, Norway

E-mail: Einar.Halvorsen@usn.no

Abstract. This paper offers insights into optimization of electret-based energy harvesters made of two patterned electrodes facing movable electret strips parallelized with a pitch p . The effective electrode dimension of such harvester structures is optimized to maximize power under given displacement amplitude and acceleration amplitude, while the length and the width of the design area are kept fixed. The geometrical optimization includes fringing field effects that may have significant impacts on the output power of the small-scale devices. The optimization problem is carried out through an established accurate lump-model represented by an equivalent circuit. The optimal electrode width that gives maximum power is proportional to the proof-mass displacement amplitude by an approximate formula $a_{\text{opt}} \approx 1.45X_0$. Optimizing the pitch can further increase the maximum power as it simultaneously regulates both optimal ratios to the electrode width and the gap size.

1. Introduction

Small-scale vibration energy generators have promoted operation of wireless sensors nodes without the need of battery by converting kinetic energy from surrounding into electrical energy. Electret-based energy harvesting is the most favourable technique with respect to the feasibility of standard microfabrication process. The use of internal bias by an electret makes the harvesters more easily self-sufficient and integrated. Recently, there are a number of harvesters structured by an electret pattern on a movable substrate and a set of metal-strip electrodes on a stationary substrate. The two substrates are separated by a micro-gap. Such harvesters have experimentally demonstrated potential applications of monitoring car-tire and windmill [1, 2].

Because of significant fringing fields in the microscale devices, an accurate harvester-model is still a challenge. There are several works in modeling and design optimization to maximize harvester performance. Their models are based on either using an ideal field assumption or time-consuming FEM computation [3, 4]. So far, there may have only an effort that investigates electrode optimization for slot-effect configured generators [5]. However, the conformal mapping technique used for the model is limited by assumption on material and geometry.

This work presents an effort to overcome the aforementioned limitations. The transducer electrodes are dimensionally optimized for power enhancement. This is accomplished by a built analytic tool that includes all possible effects of geometry, materials and fringing fields. A standard equivalent-circuit is established to capture all electromechanical dynamics as well as to numerically solve the geometrical optimization problem, based on the time-domain circuit simulator SPICE.



2. Analysis

2.1. MEMS electret-based transducer

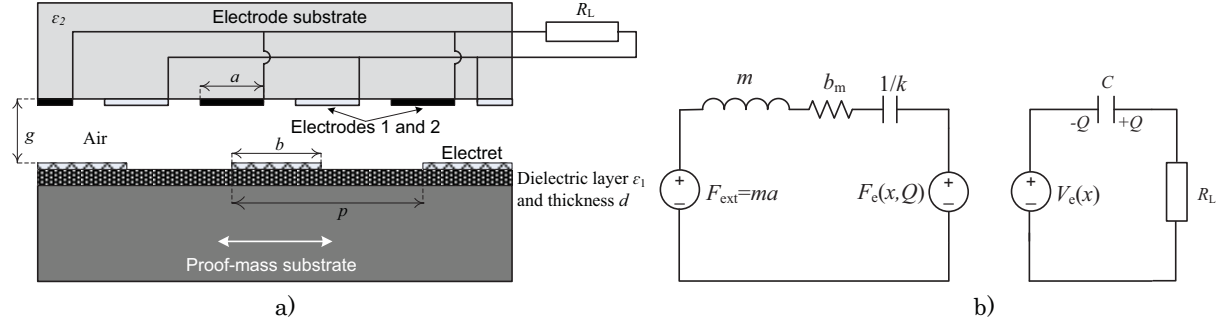


Figure 1. a) Simplified cross-section structure and b) equivalent-circuit model of an electret-based energy harvester.

A simplified cross-section of the electret-based energy transducer is shown in figure 1a. The top layer of the conductive proof-mass substrate consists of M parallel electret-strips with a width b deposited on a dielectric layer with thickness d and permittivity ϵ_1 . The electret strips distributed to each other by a pitch p symmetrically faces a set of fixed metal-electrodes 1 and 2 with width a on the top substrate with permittivity ϵ_2 by an air gap g with permittivity ϵ_0 . The proof mass m suspended by mechanical springs (not shown) with stiffness k has a relative displacement x to the two fixed-electrodes in the lateral direction. Thickness of each electrode/electret pattern is assumed negligible. The end-effects can be neglected as the period number M is considered to be sufficiently large, so that the charge distribution on each electret strip is assumed periodic and uniform. Under the proof-mass motion driven by a time-varying acceleration $a(t)$, the total fixed-charge Q_e over the entire electret induces charge variation between two fixed-electrodes, generating an electrical current through a resistive load R_L .

2.2. Equivalent-circuit model

The method used here to build an accurate model is established from our own previous work [6] that provides a fast and full exploration of design parameters. The calculation approach is essential to include all possible effects of fringing fields that may affect the output power. To this end, singular divergences of the surface charge density are taken into account at the edges of the metal strips in form of reciprocal square root. The method to calculate the all induced-charge coefficients γ_{ij} in the electrostatic system is considered as an adaption of previous boundary treatments applied for surface acoustic wave microstrip-devices [7, 8]. The total electrostatic energy stored in the system is

$$W_e = \frac{1}{2\pi\epsilon_0 ML} (\gamma_{12}Q_1Q_2 + \gamma_{13}Q_1Q_e + \gamma_{23}Q_2Q_e) + \frac{1}{4\pi\epsilon_0 ML} (\gamma_{11}Q_1^2 + \gamma_{22}Q_2^2 + \gamma_{33}Q_e^2) \quad (1)$$

where Q_1 and Q_2 are the total charges on the electrodes 1 and 2, and L is the electrode length. The induced-charge coefficients depend on the transducer geometry, the material properties and the relative displacement x . Further details of the coefficient calculation γ_{ij} can be found in [6].

The electromechanical transducer can be now represented by an equivalent-circuit based on the $e \rightarrow V$ convention [9, 10] in figure 1b, where b_m is the mechanical damping coefficient and $F_{\text{ext}} = ma$ is the external force. In the circuit, three key elements $F_e(x, Q)$, $V_e(x)$ and C are

$$F_e(x, Q) = \frac{\partial W_e}{\partial x} = \frac{\gamma'_{33}(x) - \frac{4\pi d}{\epsilon_1 p(\gamma_{11} - \gamma_{12})} [\gamma'_{13}(x) + \gamma'_{23}(x)]}{4\pi\epsilon_0 ML} Q_e^2 + \frac{\gamma'_{13}(x) - \gamma'_{23}(x)}{2\pi\epsilon_0 ML} Q_e Q \quad (2)$$

and

$$V_e(x) = \frac{\gamma_{13}(x) - \gamma_{23}(x)}{2\pi\epsilon_0 ML} Q_e, \quad C = \frac{\pi\epsilon_0 ML}{\gamma_{11} - \gamma_{12}}. \quad (3)$$

where $Q = \frac{Q_1 - Q_2}{2}$. The force $F_e(x, Q)$ represents the electromechanical coupling between mechanical and electrical domains of the transducer, the displacement-dependent built-in source $V_e(x)$ is the open-circuit voltage when $Q = 0$ and C is the effective capacitance between the two electrodes 1 and 2.

3. Electrode optimization

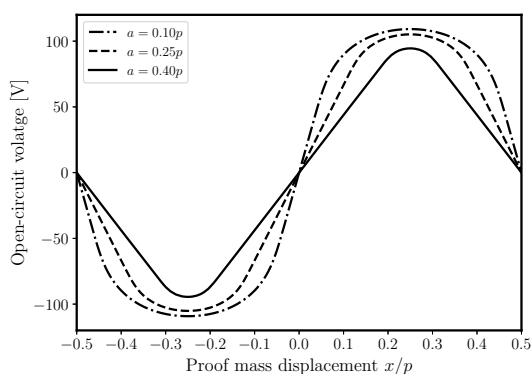


Figure 2. Open-circuit voltage vs. proof mass displacement for different metallization ratios a/p .

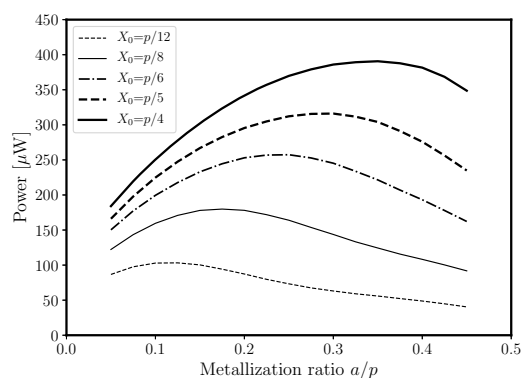


Figure 3. Output power as a function of metallization ratio for different amplitudes of proof mass displacement.

In order to optimize the electrode dimension of the transducer, the active design area is kept fixed during the optimization which seeks an effective electrode area that gives maximum power for given displacement amplitude X_0 or acceleration amplitude A . All design parameters are taken from the device example in [3], except a and p that are the dimension parameters to be optimized. The device had a set of Si_3N_4 electret strips on the SiO_2 dielectric layer deposited on the silicon proof mass substrate. The substrate for the metal-electrodes makes use of glass material. The design area is $10 \times 10 \text{ mm}^2$.

Figure 2 shows open-circuit voltages for different metallization ratios $0 < a/p < 0.5$. The maximum voltage-amplitude at $|x/p| = 0.25$ is higher for the lower ratio a/p , but the linear range is extended for larger electrode. With short electrode, the voltage rate decreases for the displacement $|x/p| \rightarrow 0.25$. It can be explained that the induced charges on the two electrodes have less variation when one of the electrodes completely overlaps the electret pattern. The voltage amplitude increases for decreasing a/p , but the effective capacitance C is correspondingly reduced for example $C = 11.3 \text{ pF}$ for $a/p = 0.1$ and $C = 31.5 \text{ pF}$ for $a/p = 0.4$. The higher ratio a/p is required to maximize power for the larger amplitude X_0 under load optimization, see Figure 3. For $X_0 = p/12$, a maximum power is obtained at an optimal electrode $a_{\text{opt}} = 0.12p$ while this value is of $a_{\text{opt}} = 0.35p$ at $X_0 = p/4$. The relation of a_{opt} to X_0 can be approximated by a linear fit in figure 4. The optimal electrode width is approximately $a_{\text{opt}} \approx 1.45X_0$, so that the optimization is achieved when the displacement reaches two extremes of the linear range. The device parameters used for the lumped-model here have $d/p = 2 \times 10^{-3}$ and $g/p = 2 \times 10^{-2}$, but this optimal condition can be generalized to various geometries with $d \ll g < p$ for the similar MEMS harvester structures.

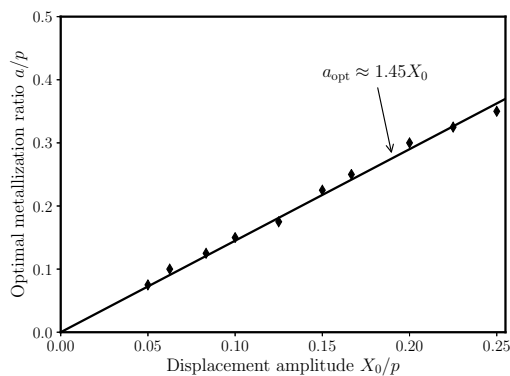


Figure 4. Relationship between optimal electrode width a_{opt} and displacement amplitude X_0 .

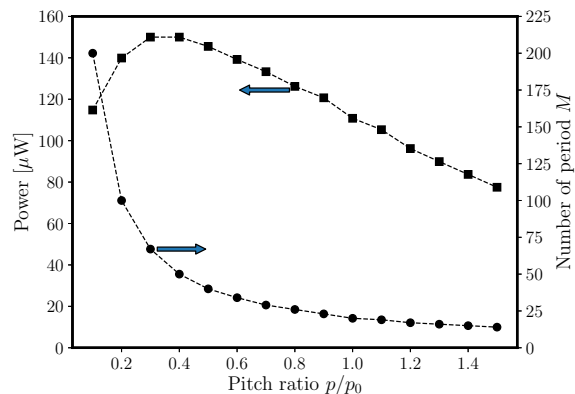


Figure 5. Output power and number of period as a function of pitch p for $p_0 = 500 \mu\text{m}$, $A = 2.0 \text{ g}$ and $a/p = 0.4$.

Figure 5 shows an alternative to optimize electrode area by varying the pitch p while keeping $a/p = 0.4$ fixed. Increase of M when scaling p down causes stronger electrostatic force, leading to smaller X_0 at the same acceleration amplitude. The maximum power achieved at $p/p_0 = 0.3$ is about 1.08 times higher than that obtained by only optimizing a/p ($a_{\text{opt}} = 0.15p$) at $p/p_0 = 1.0$. It is because the change of the pitch makes the ratio g/p further optimized while the condition $a = a_{\text{opt}}$ is still ensured by impedance matching which affects X_0 . The same maximum power is obtained at optimal load when varying both a/p and p/p_0 .

4. Conclusion

We investigated geometrical optimization for the eletret-based vibration energy harvester configured in the slot-effect scheme. The optimization problem is to explore an effective electrode area for maximizing the harvested power with respect to the constraint of the total design area. To build a simulation tool, an accurate lumped-model that governs both the electromechanical dynamics and the fringing field effects was established in form of the standard equivalent circuit. The optimal electrode is found to be proportional to the proof-mass displacement amplitude by a linear approximation $a_{\text{opt}} \approx 1.45X_0$, while the pitch optimization is possible to enhance a higher maximum power.

Acknowledgments

This work was supported by the Research Council of Norway through the Grant no. 229716/E20.

References

- [1] Renaud M, Altena G et al. 2013 *Proc. Transducer2013, (Barcelona, June)*, 693–696
- [2] Perez M, Boisseau S et al. 2016 *Smart Mater. Struct.* **25** 045015
- [3] Renaud M, Altena G et al. 2015 *Smart Mater. Struct.* **24** 085023
- [4] Crovetto A, Wang F and Hansen O 2014 *J. Microelectromechanical Systems* **23** 1141–1155
- [5] Okamoto H, Hamate Y and Kuwano H 2012 *Smart Mater. Struct.* **21** 065001
- [6] Le C P and Halvorsen E 2017 *Smart Mater. Struct.* **26** 085042
- [7] Gladwell G M L and Coen S 1975 *IEEE Trans. Microwave Theory Tech.* **23** 865–870
- [8] Medina F and Horno M 1992 *IEEE Trans. Microwave Theory Tech.* **40** 1748–1756
- [9] Tilmans H A C 1996 *J. Miromech. Miroeng.* **6** 157–176
- [10] Jezierski E 2001 *Proc. Workshop Robot Motion and Control (Bukowy Dworek, Poland, October)* 181–188.